Supplement of Atmos. Meas. Tech., 8, 1701–1718, 2015
http://www.atmos-meas-tech.net/8/1701/2015/
doi:10.5194/amt-8-1701-2015-supplement

Atmospheric Measurement Techniques
Open Access

Supplement of

Assessment of the sensitivity of core / shell parameters derived using the single-particle soot photometer to density and refractive index

J. W. Taylor et al.

Correspondence to: J. W. Taylor (jonathan.taylor@manchester.ac.uk)

S1. SP2 calibrations

Glassy carbon spheres were nebulised, drawn through a diffusion drier and size-selected using a differential mobility analyser (DMA). Monodisperse sizes between 80-500 nm mobility diameter spanned the dynamic range of the instrument. A power law fit was used to relate glassy carbon diameter to SP2 detector response, and particle mass was calculated using an assumed density of glassy carbon of 1.42 gcm^{-3} (Slowik et al., 2007). Ambient particle mass-equivalent diameter was calculated assuming a core density, ρ_C, of 1.8 gcm^{-3} (Bond and Bergstrom, 2006). The exponents of the power law fit were 0.34 and 0.36 for the broadband and narrowband detectors. An exponent of 1/3 corresponds to a linear fit vs particle mass; the small deviation from this value is likely due to the nonlinearity of the SP2 for large masses (Moteki and Kondo, 2010). Repeated calibrations showed that the response of the incandescence channels was stable to within ±2% during the course of the experiment.

The per-particle uncertainty in mass measurement is 30% (Schwarz et al., 2008a; Shiraiwa et al., 2008). The statistical uncertainty in rBC mass concentration for each 5-minute averaging period was ~2.5%. There is also likely a systematic error in bulk rBC mass concentration due to the test aerosol used (Laborde et al., 2012a). To assess the impact of this, Manchester's SP2 was compared to the NOAA SP2 (Perring et al., 2011), which was calibrated using fullerene soot. Both instruments sampled from three Teflon bags containing different sizes of monodisperse fullerene soot, in the same intercomparison described by Metcalf et al. (2012). rBC modal mass measured by Manchester's SP2 was approximately 10% higher than that reported by the NOAA instrument when comparing several sizes of monodisperse fullerene soot (Anne Perring, private communication, 2012). Convolving this value with the 10% uncertainty due to the SP2's response to fullerene soot relative to diesel (Laborde et al., 2012a) gives a systematic uncertainty estimate of average rBC per-particle mass of ±14%, which corresponds to a difference in derived core diameter of $^{+4.5\%}_{-4.9\%}$. Assuming any error due to flow calibration is negligible, the error on the derived rBC mass concentration was also ±14%.

The SP2 also uses avalanche photodiodes (APDs) to measure light scattered by particles as they pass through the beam. One APD is position-sensitive, allowing measurement of the position of a particle as it passes through the laser (Gao et al., 2007). This is necessary for calculating the size of a coated BC-containing particle before it begins to vaporise. Calibrations of the scattering channels were performed periodically with polystyrene latex spheres (PSLs; Thermo Fisher Scientific, Waltham, MA, USA) 90-500 nm in diameter, and showed the response was stable to within 3% throughout the experiment. No systematic time or temperature dependence in the scattering response was observed. PSLs were also used to ensure proper alignment of the particle jet with the laser beam (SP2 operator manual, 2007).

Prior to 2150UTC on 18 May, the SP2's laser power was deemed insufficient to fully quantify the rBC mass concentration, based on a careful analysis of initial calibration data. The laser power was increased and data obtained using the lower laser power were discarded. The higher laser intensity was deemed high enough to properly detect rBC mass using the colour ratio method described by (Schwarz et al., 2010).

The SP2 only records a particle when either the scattering or broadband incandescence detector voltages increase above a certain threshold, and cannot record another until it drops back below. The SP2 data acquisition software used at the time (version 2.9.4) calculated the threshold using a user-defined level above the baseline. During some periods the scattering threshold would be set too low or high, rendering the instrument unable to record particles, and causing the recorded concentrations to be artificially low. These data were filtered on a 10-second time basis by removing extreme outliers, defined as periods where the rBC number concentration was less than three interquartile ranges below the lower quartile for each 10-minute sampling period. This filtered out 0.8% of the 10s data when the auto-thresholding was used. After 2150 on 19 May, the auto-thresholding was disabled and the trigger threshold held constant. No time-dependent variations in the broadband incandescence threshold were observed, so this did not affect the measured rBC concentration.

S2. rBC core size distribution

The campaign average volume-equivalent D_C distribution is shown in Figure S1. While the distribution showed some variation throughout the campaign, this was relatively minor. The average distribution was nearly identical through the thermodenuder, meaning charring is unlikely to have affected the particles. The peak position at 130 nm is close to that reported by Metcalf et al. (2012) in the LA basin during May 2010, and other previous measurements of fresh diesel emissions (McMeeking et al., 2010; Laborde et al., 2012b). Liggio et al. (2012) reported a mass mode of 145 nm during relatively high Heavy-Duty Diesel Vehicle (HDDV) period in Toronto, though they calibrated their instrument with Aquadag. Accounting for the 40% difference in instrument response between Aquadag and ambient soot (Laborde et al., 2012a) gives excellent agreement between the peak positions.

Liggio et al. (2012) also observed the tail of a distribution that peaked at D_C < 75 nm, which they attributed to gasoline emissions, which was not seen in Pasadena. This provides further evidence that diesel emissions are responsible for the majority of black carbon measured during CalNex.

A smaller secondary mode, with peak at 450 nm, is also evident, however using the Gaussian fits this mode was calculated to contain only 5% of rBC mass. This second mode may be due to local emissions, coagulated diesel recirculated within the LA basin, or long-range transport.

Based on the lognormal fits, the fraction of rBC mass outside the detection range of the SP2 was estimated as 4.6% of the total. rBC mass concentration measured by the SP2 was corrected for this factor.

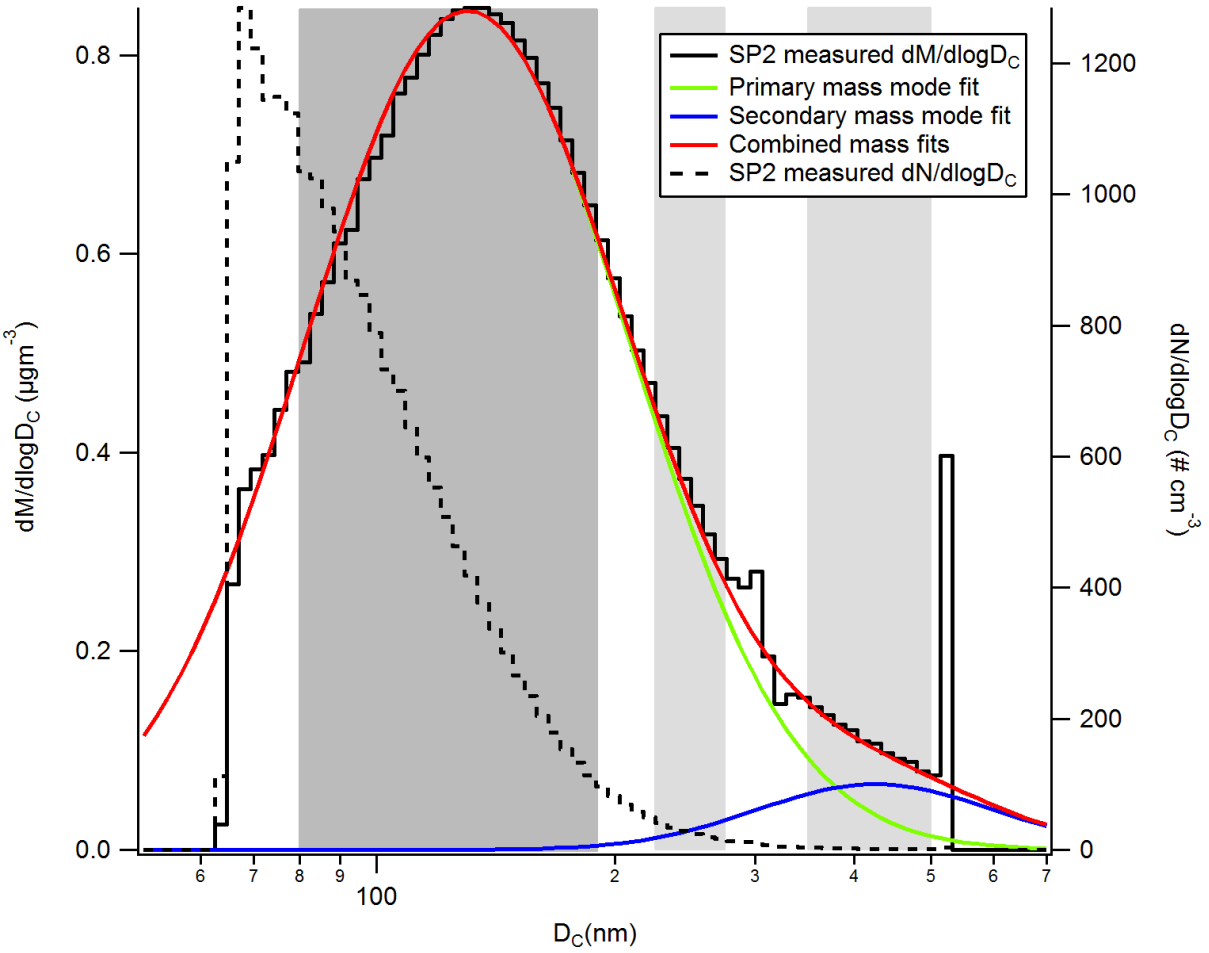

Figure S1 - Average rBC mass-equivalent core diameter mass and number distributions measured by the SP2 during CalNex. A lognormal distribution was fit to dM/dlogD_C in the dark grey region. This fit was then subtracted from the measured data, and a second lognormal distribution was fit to the residual data in the light grey region. The discontinuity around 330 nm is due to the switch in detectors as the narrowband detector reached saturation, and was not used for the fits. The centres of the fitted modes and lognormal widths were 130 nm ± 23% and 426 nm ± 41%.

S3. Black/Elemental carbon instrument comparison

S3.1. Sunset OC/EC analyser

The Sunset OC/EC analyser (Birch and Cary, 1996) is widely used for measuring Elemental Carbon (EC). The specific instrumental setup during CalNex was described by Zhang et al. (2011). Data were reported on an hourly basis, representing the average of the first 44 minutes of each hour.

The instrument reports two separate calculations of EC, one based on the NIOSH 5040 thermal protocol (Birch, 2002) (which we refer to as EC_{Sun}) and the other referred to as "optical EC" (Jeong et al., 2004). Laser attenuation through a filter is defined as $ATN = \ln(I_{Loaded}/I_{Blank})$, where I_{Loaded} and I_{Blank} are the measured laser powers through a loaded and blank filter respectively.

The concentration of elemental carbon embedded per unit area ([*EC*], μgcm^{-2}), is then calculated by $[EC] = ATN/\sigma$, where σ is the attenuation coefficient. This is a function of the aerosol embedded on the filter, due to filter loading and scattering artefacts, similar to those in other filter-based absorption measurements (e.g. Cappa et al., 2008; Lack et al., 2008; Coen et al., 2010). Rather than explicitly correcting for these artefacts individually, σ is calculated by the empirically-derived relationship (David Smith, Sunset Laboratories, Private communication, 2012) $\sigma = (0.75 \times ATN + 2.25)^{-1}$. [*EC*] is then divided by the total flow through the filter during each sampling period, corrected for difference in units, to yield the mass concentration in μgm^{-3}. Due to the optical nature of the measurement, Jeong et al. (2004) considered this as a measure of black, rather than elemental, carbon and we adopt their notation in referring to the "optical EC" mass concentration as BC_{Sun}. Total carbon concentration (*TC*) is only measured by the thermal method.

For most of the experiment, the OC/EC analyser was sampling through a $PM_{2.5}$ cyclone. During several periods during 12th-15th June, the instrument switched periodically between a $PM_{2.5}$ and PM_1 cyclone. Based on this comparison, it is estimated around 7% of the BC_{Sun} mass was contained in particles greater than 1μm in diameter.

S3.2. SP2/Sunset comparison

Figure S2a shows an excellent correlation between rBC mass concentration measured by the SP2 and BC_{Sun}, indicating both are measuring the same quantity. This is an important distinction, as rBC, BC_{Sun} and EC_{Sun} are all operationally defined, and may be similar but fundamentally different quantities on a physical and chemical level (Andreae and Gelencser, 2006). The ratio between the two shows agreement within 20%, though the Sunset instrument was measuring on a $PM_{2.5}$ inlet, which accounts for some of this difference. Accounting for the 7% fraction of supermicron BC_{Sun} during CalNex leaves a difference of 14% (Hayes et al., 2013). Whilst this may indicate greater losses in the SP2 sampling system, this does not affect calculation comparison of the BC instruments which used the same inlet. Other explanations are also possible, such as the calibration of either instrument.

Nevertheless, the excellent correlation between rBC and BC_{Sun} warrants further study to see if this is consistent in different environments.

Figure S2b shows the correlation between rBC and EC_{Sun}, which is weaker than that with BC_{Sun}. This suggests that while the two are clearly from the same source, the relationship between the two shows more variation. Multiple factors are likely involved. Errors in measurement of blank filters affect both Sunset measurements, and increased organic loadings cause interference, for BC_{Sun} due to increased scattering artefacts, and for EC_{Sun} due to changes in thermogram properties.

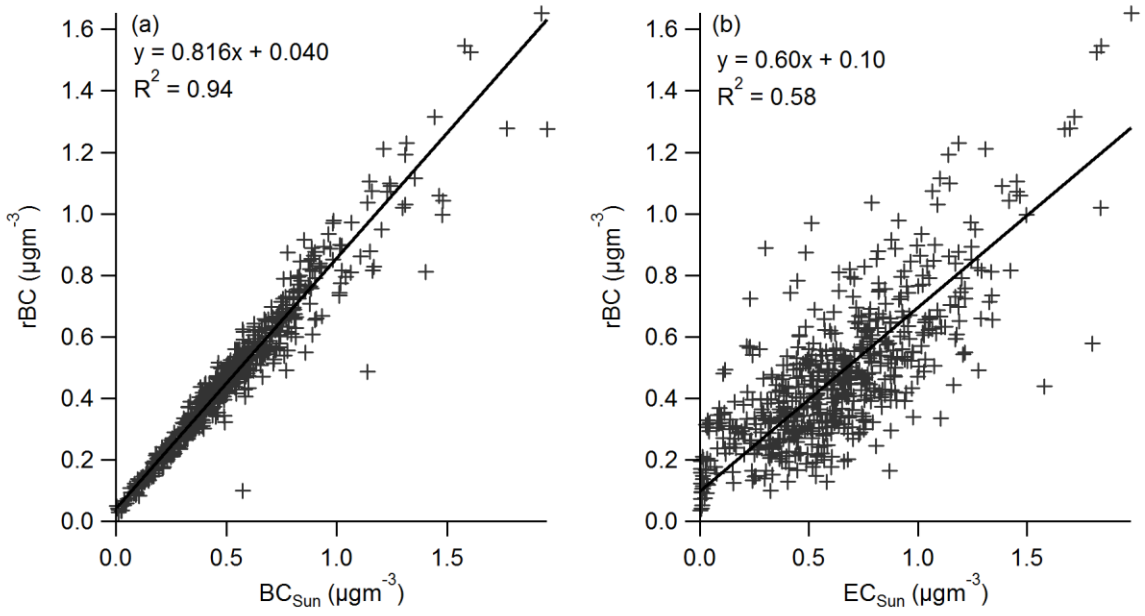

Figure S2 – Comparison between the SP2 and Sunset instruments. Panels (a) and (b) show the correlation between rBC and Sunset BC_{Sun} and EC_{Sun} respectively. The black lines are orthogonal distance regression fits to the data.

S3.3. SP2/SP-AMS comparison

The sensitivity of the SP-AMS rBC collection efficiency to SP-AMS inorganic mass concentration is presented in Figure S3. When inorganics were higher, the ratio of SP-AMS rBC to SP2 rBC was also higher. As the SP2 rBC measurement is insensitive to nonrefractory species (Moteki and Kondo, 2007), this behaviour must be due to the SP-AMS.

An explanation for this behaviour is that the SP-AMS was not detecting the smaller, fresher particles through them not efficiently hitting the laser beam. The SP-AMS particle time-of-flight size distributions, shown in Figure S4, demonstrate that inorganics were indicative of a shift in rBC particle diameter to larger particles. The difference between Figs. S4 and S1 is that the SP-AMS measures coated particle diameter, rather than core diameter. The rBC size distribution shown in Figure S4 is therefore dependent not only on the amount of rBC per particle, but also on the amount of coating.

Unlike the standard AMS, the particle beam of the SP-AMS has a much smaller target to hit to become detected (a <1 mm laser as opposed to a 3 mm vaporiser) (Onasch et al., 2012). As such, this makes the SP-AMS much more sensitive to the width of the particle beam (Huffman et al., 2005) and smaller, particles may not be sufficiently focused to be detected efficiently. Note that because of signal-to-noise considerations, the lens alignment is normally performed with larger (~300nm) particles.

Another possible sensitivity is to particle shape, as more fractal particles are focused less efficiently through the aerodynamic lens (Huffman et al., 2005). If condensation of secondary inorganics caused a collapse of fractal soot structure, and this was determining the collection efficiency, similar results would be seen for the ambient and thermodenuded data. However, the thermodenuded data in Figure S3 only a weak dependence on ambient inorganics, meaning overall particle size was more important.

Compared to Cappa et al. (2012), there will have been a generally greater fraction of fresher particles in Pasadena, however the apparent discrepancy in performance may also be due to physical differences between the instruments. The AMS chamber used here was the longer 255 type (395 mm between nozzle and ioniser) as opposed to the 215 type used by Cappa et al. (2012) (295 mm), which would worsen any focusing problems in this study. However, it is also possible that the aerodynamic lens was under-performing, for example due to loose or misaligned internal components, which can cause particle of different sizes to focus in different directions.

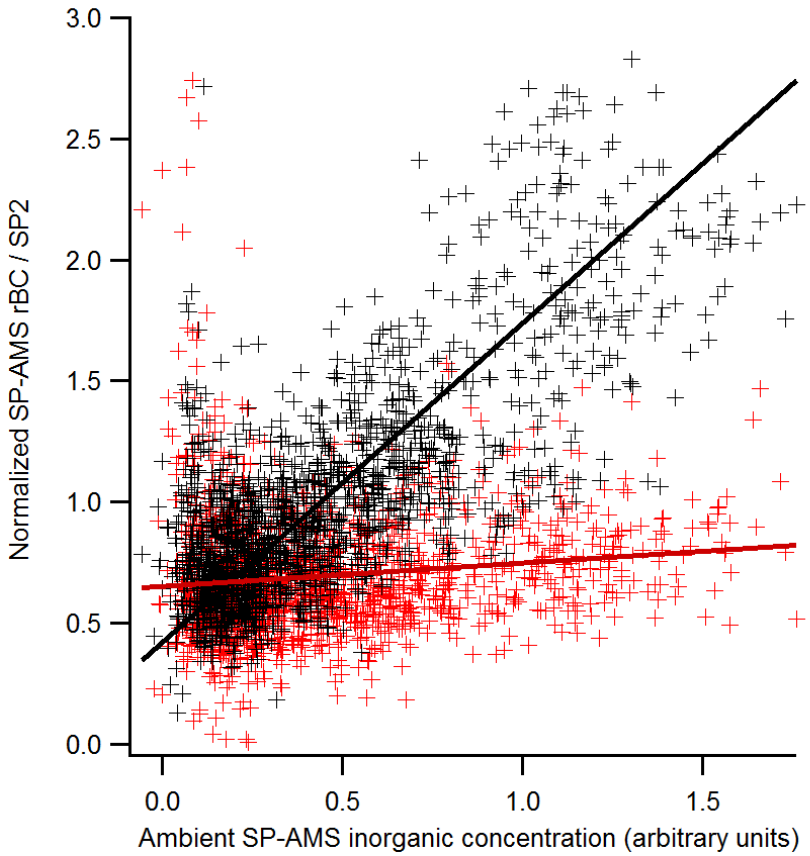

Figure S3 – Comparison of the SP-AMS and SP2 rBC mass concentrations, for ambient (black) and thermodenuded (red) rBC data, compared to the ambient inorganic concentration measured by the SP-AMS. The y-axis is normalized to the average ambient ratio, as only the relative changes are meaningful.

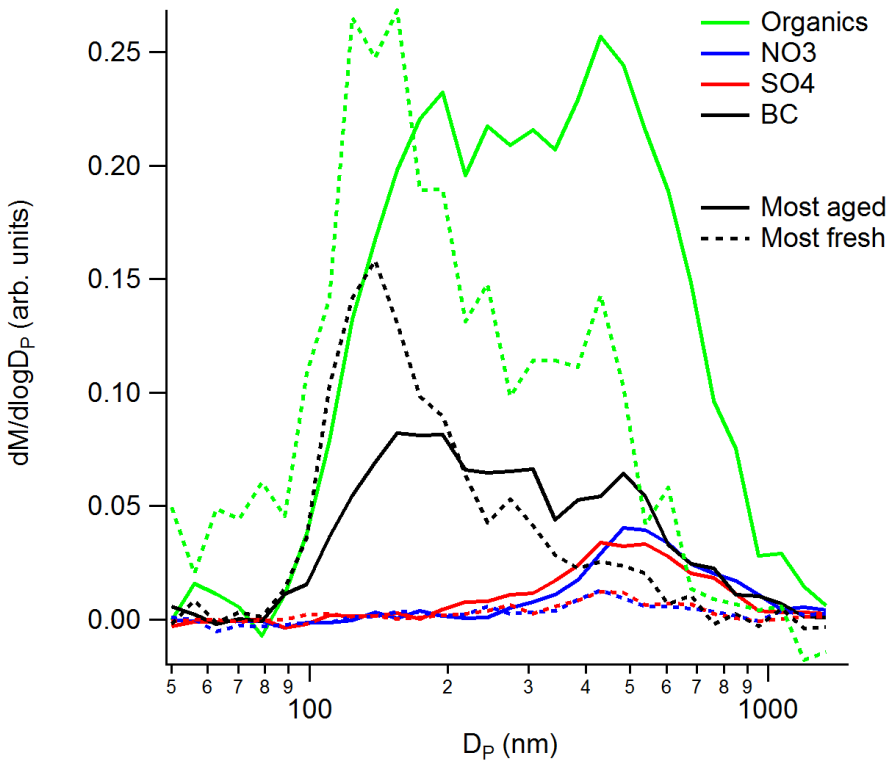

Figure S4 – Size distribution of coated particles' vacuum aerodynamic diameter measured by the SP-AMS. The most aged particles are defined as those measured when –log(NOx/NOy) was >90th percentile (0.34), and the most fresh when –log(NOx/NOy) was < 10th percentile (0.08). rBC and organics showed a bimodal distribution, suggesting smaller primary particles and secondary coating growth. Inorganics were present only in larger particles, and rBC was contained in larger particles when they were present.

S4. Thermodenuded composition

A thermogram of the different species measured by the SP-AMS is presented in Figure S5. We note that this plot represents the average for the whole campaign, as the signal/noise was not high enough to split into different photochemical ages. The volatility of species is similar to those in Riverside, CA (Huffman et al., 2009), though we did not see the apparent enhancement in SO_4 at 80-140 °C that they observed. This was thought to be due to a phase change in the sulphate causing increased collection efficiency in the heater. As the SP-AMS does not have a heater, this result may support their hypothesis; SO_4 was however enhanced compared to SP-AMS rBC.

As all the data are normalised to the SP2 rBC mass fraction remaining, which we consider to be reliable, it is not immediately clear why the SP-AMS rBC mass fraction decreases with temperature, and is <1. This may be due to the removal of semi-volatile material causing a change in particle size and shape, which affected the transmission of particles through the aerodynamic lens, and hence reduced the collection efficiency.

The fractional composition at different thermodenuder temperatures is shown in Figure S6a. Even at the highest temperatures, only 35% of mass is contained in the C_X rBC fragments. This may appear to show that particles were still significantly coated, but there are two reasons that this is unlikely to be the case. Firstly, as rBC measured by the SP-AMS was biased low compared to the SP2, and this was most significant at higher temperatures, the true C_X fraction is probably higher. Secondly, Figure S6b shows the organic mass spectrum at these temperatures. The majority of organic aerosol was composed of the CO_2^+ ion and associated fragments, with the remaining spectrum typical of Hydrocarbon-like Organic Aerosol (HOA). Onasch et al. (2012) reported a CO_2^+ fragment in the flame soot spectrum that was not measured with the laser off, suggesting it may due to be some form of refractory oxygenated soot. For this dataset the SP-AMS was run with the heater off, so we are unable to confirm that this CO_2^+ is refractory, but if this were the case, it would be more appropriate to think of this as rBC rather than organic, as suggested by Corbin et al. (2014).

If all the CO_2^+ fragments were associated with rBC, the ratio of CO_2^+/rBC would hold constant for the entire dataset. Conversely, if the CO_2^+ was entirely organic, the CO_2^+ fraction would depend only on organic composition. In reality the data is probably somewhere between these two cases, but at the hottest thermodenuder temperatures the CO_2^+ fraction is significantly higher than is typical of even the most oxygenated organics (Ng et al., 2010). This, combined with the reduced C_X collection efficiency through the thermodenuder (shown in Fig. S3), demonstrates that it is likely that at the hottest thermodenuder temperatures, the majority of non-rBC material was removed.

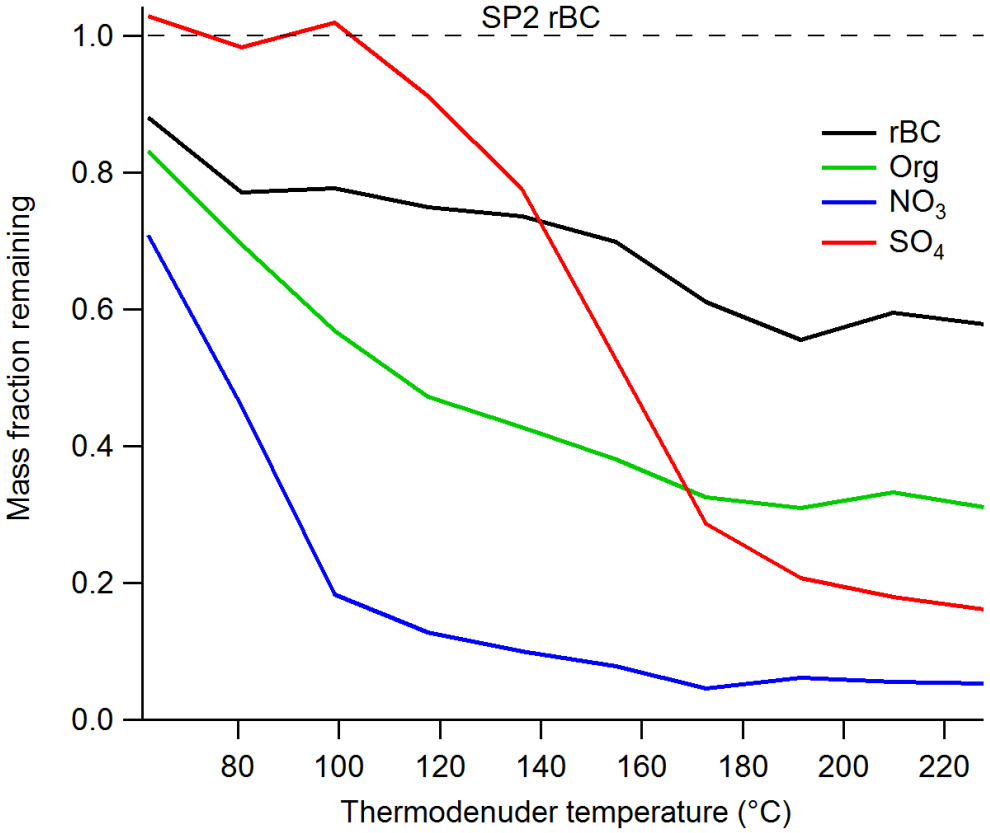

Figure S5 – Campaign average thermodenuded mass fraction remaining, compared to ambient measurements, of species measured by the SP-AMS. Data have been corrected for thermophoretic losses by normalising to the SP2 rBC mass fraction remaining at the relevant temperature.

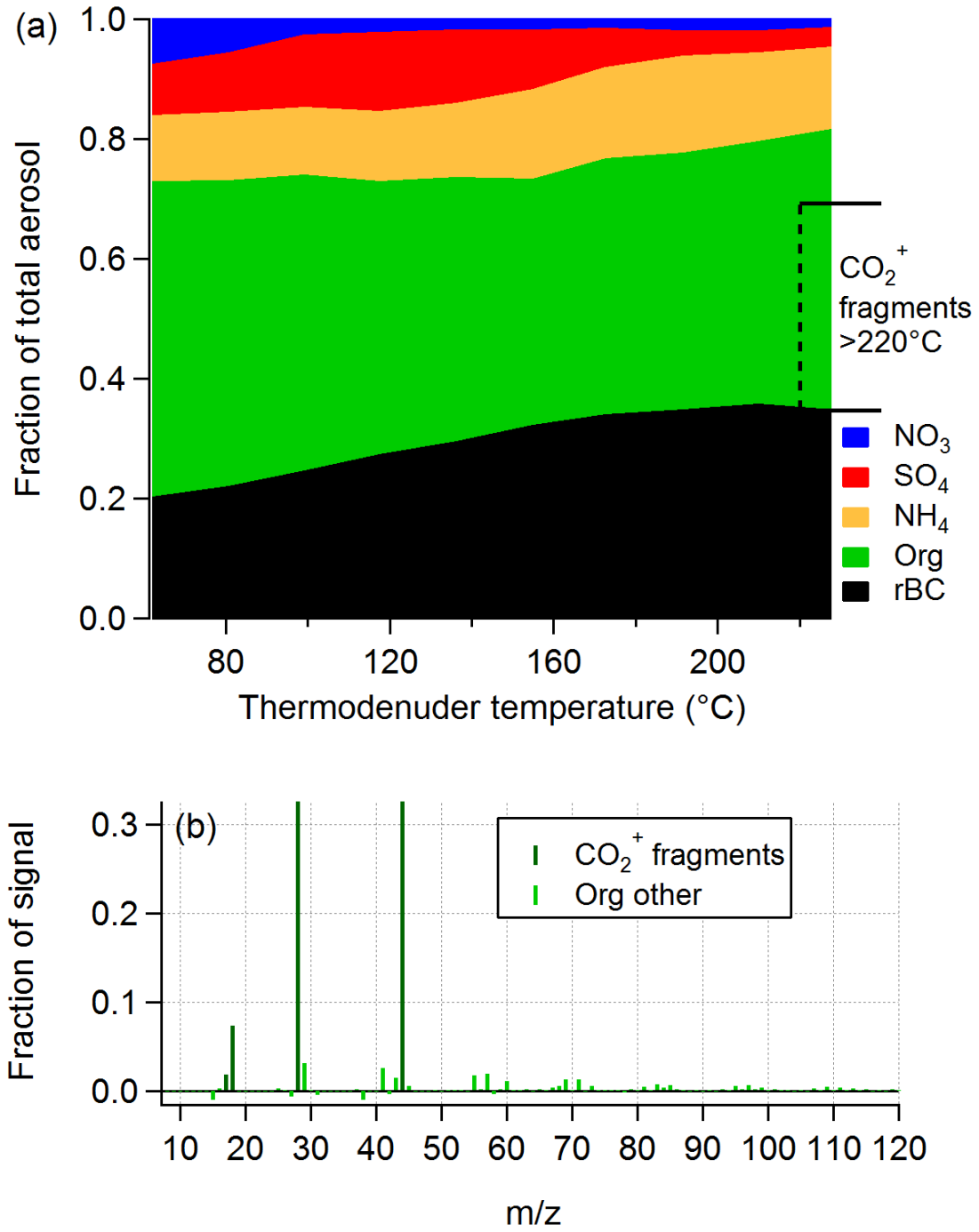

Figure S6 – (a) shows the fractional contributions to thermodenuded SP-AMS mass at different temperatures, and (b) the organics mass spectrum through the thermodenuder at temperatures >220°C. At these temperatures, 74% of organics are associated with the CO_2^+ fragment.

S5. Removal of primary coatings

Figure S7 shows a thermogram of the median E_{Sca} taken under the freshest ambient conditions. For temperatures <180°C, there is a trend of decreasing E_{Sca} with increasing temperature, suggesting the presence of some primary coating that was removed at higher temperatures. However, above 180°C there is no significant trend, meaning above this temperature, any primary coatings were removed, leaving BC that could reasonably be considered externally-mixed. By considering only data the freshest airmasses, we minimise the effects of any coating material the thermodenuder would not be able to remove.

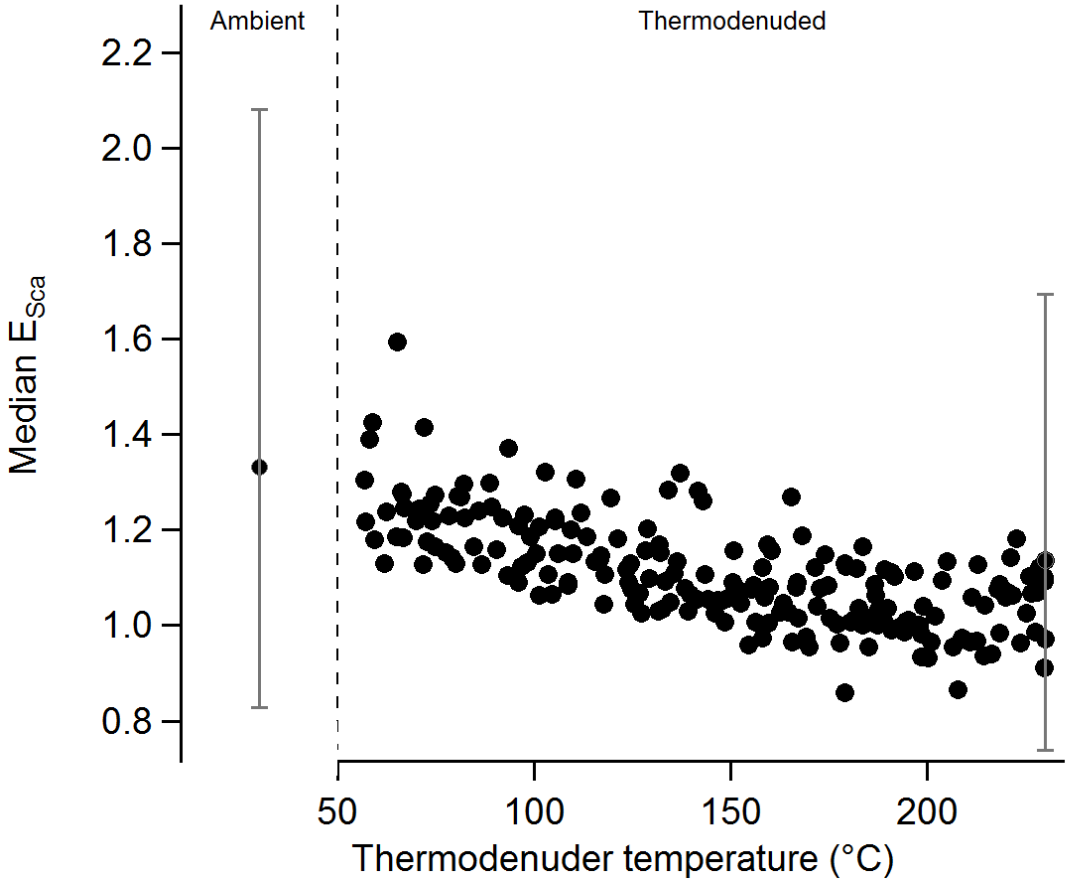

Figure S7- Median E_{Sca}, from the freshest ambient airmasses, as a function of thermodenuder temperature. The average for ambient data in the same atmospheric conditions is shown for comparison. The data were calculated using, calculated using $n_C = (2.26 - 1.26i)$ and ρ_C = 1.8 gcm^{-3} and are only take from particles with 135 ≤ D_C ≤ 200 nm. The data are 5-minute averages, and are all taken from the periods defined as the freshest ambient conditions (-log(NO_X/NO_Y) < 10th percentile). The grey error bars show the 25th and 75th percentiles of selected data points, to demonstrate the spread in the data.

S6. Summary of ρ_C and n_C used in previous ambient SP2 core/shell studies

Previous publications studying ambient SP2 core/shell data have followed Bond and Bergstrom's recommendations to varying degrees. Langridge et al. (2012) and Metcalf et al. (2012) used the highest refractive index recommended and the density in the middle of the range, whilst Subramanian et al. (2010) used the same refractive index but a higher density.

Shiraiwa et al. (2008) based their density ρ_C = 1.77 gcm^{-3} on denuded aerosol particle mass analyzer (APM) measurements of diesel soot. They explored the sensitivity of scattering cross section to core refractive index for graphite particles, but when modelling ambient data they used refractive indices for carbon black. Citing three measured values, they settled on the central value of $n_C = (1.87 - 0.56i)$ and estimated a 20% error in calculated absorption coefficient between the different values.

Schwarz et al. (2008a, 2008b, 2009) used a density ρ_C = 2 gcm^{-3} and refractive index of $n_C = (2 - 1i)$, to match that derived by Schnaiter et al. (2005) by comparing diesel soot size distributions to measured bulk optical properties, using a fractal particle model. They briefly investigated the effect of core refractive index and found little sensitivity to calculated absorption enhancement, though they calculated this at 1064 nm rather than a visible wavelength.

Unlike the other studies discussed, Kondo et al. (2011) and Moteki et al. (2012) focused on biomass burning aerosol, while Sahu et al. (2012) measured both fossil fuel and biomass burning emissions. They matched their refractive index and density to those used in the optical properties of aerosols and clouds (OPAC) software package (Hess et al., 1998), giving a density ρ_C = 2 gcm^{-3} and refractive index of $n_C = (1.76 - 0.44i)$. They also used the SP2's scattering channel, at the onset of incandescence, to estimate the rBC core diameter, rather than using the incandescence channel. We investigated this method, but did not observe a clear scattering cross section of the rBC core, as shown in Laborde et al. (2012a), and use the incandescence channel to reduce ambiguity.

References

Andreae, M. O. and Gelencser, A.: Black carbon or brown carbon? The nature of light-absorbing carbonaceous aerosols, Atmos. Chem. Phys., 6, 3131–3148, 2006.

Birch, M. E.: Occupational monitoring of particulate diesel exhaust by NIOSH method 5040, Appl. Occup. Environ. Hyg., 17, 400–405, doi:10.1080/10473220290035390, 2002.

Birch, M. E. and Cary, R. A.: Elemental carbon-based method for monitoring occupational exposures to particulate diesel exhaust, Aerosol Sci. Technol., 25, 221–241, doi:10.1080/02786829608965393, 1996.

Bond, T. C. and Bergstrom, R. W.: Light absorption by carbonaceous particles: An investigative review, Aerosol Sci. Technol., 40, 27–67, doi:10.1080/02786820500421521, 2006.

Cappa, C. D., Lack, D. A., Burkholder, J. B. and Ravishankara, A. R.: Bias in filter-based aerosol light absorption measurements due to organic aerosol loading: Evidence from laboratory measurements, Aerosol Sci. Technol., 42, 1022–1032, doi:10.1080/02786820802389285, 2008.

Cappa, C. D., Onasch, T. B., Massoli, P., Worsnop, D. R., Bates, T. S., Cross, E. S., Davidovits, P., Hakala, J., Hayden, K. L., Jobson, B. T., Kolesar, K. R., Lack, D. A., Lerner, B. M., Li, S.-M., Mellon, D., Nuaaman, I., Olfert, J. S., Petaja, T., Quinn, P. K., Song, C., Subramanian, R., Williams, E. J. and Zaveri, R. A.: Radiative Absorption Enhancements Due to the Mixing State of Atmospheric Black Carbon, Science (80-.)., 337, doi:10.1126/science.1223447, 2012.

Coen, M. C., Weingartner, E., Apituley, A., Ceburnis, D., Fierz-Schmidhauser, R., Flentje, H., Henzing, J. S., Jennings, S. G., Moerman, M., Petzold, A., Schmid, O. and Baltensperger, U.: Minimizing light absorption measurement artifacts of the Aethalometer: evaluation of five correction algorithms, Atmos. Meas. Tech., 3, 457–474, 2010.

Corbin, J. C., Sierau, B., Gysel, M., Laborde, M., Keller, A., Kim, J., Petzold, A., Onasch, T. B., Lohmann, U. and Mensah, A. A.: Mass spectrometry of refractory black carbon particles from six sources: carbon-cluster and oxygenated ions, Atmos. Chem. Phys., 14(5), 2591–2603, doi:10.5194/acp-14-2591-2014, 2014.

DMT: Single Particle Soot Photometer (SP2) - Operator Manual, Revision 1.5, Droplet Measurement Technologies., 2007.

Gao, R. S., Schwarz, J. P., Kelly, K. K., Fahey, D. W., Watts, L. A., Thompson, T. L., Spackman, J. R., Slowik, J. G., Cross, E. S., Han, J.-H. H., Davidovits, P., Onasch, T. B. and Worsnop, D. R.: A Novel Method for Estimating Light-Scattering Properties of Soot Aerosols Using a Modified Single-Particle Soot Photometer, Aerosol Sci. Technol., 41(2), 125–135, doi:10.1080/02786820601118398, 2007.

Hayes, P. L., Ortega, A. M., Cubison, M. J., Froyd, K. D., Zhao, Y., Cliff, S. S., Hu, W. W., Toohey, D. W., Flynn, J. H., Lefer, B. L., Grossberg, N., Alvarez, S., Rappenglück, B., Taylor, J. W., Allan, J. D., Holloway, J. S., Gilman, J. B., Kuster, W. C., de Gouw, J. A., Massoli, P., Zhang, X., Liu, J., Weber, R. J., Corrigan, A. L., Russell, L. M., Isaacman, G., Worton, D. R., Kreisberg, N. M., Goldstein, A. H., Thalman, R., Waxman, E. M., Volkamer, R., Lin, Y. H., Surratt, J. D., Kleindienst, T. E., Offenberg, J. H., Dusanter, S., Griffith, S., Stevens, P. S., Brioude, J., Angevine, W. M. and Jimenez, J. L.: Organic aerosol composition and sources in Pasadena, California, during the 2010 CalNex campaign, J. Geophys. Res. Atmos., 118(16), 9233–9257, doi:10.1002/jgrd.50530, 2013.

Hess, M., Koepke, P. and Schult, I.: Optical properties of aerosols and clouds: The software package OPAC, Bull. Am. Meteorol. Soc., 79, 831–844, doi:10.1175/1520-0477(1998)079<0831:opoaac>2.0.co;2, 1998.

Huffman, J. A., Docherty, K. S., Aiken, A. C., Cubison, M. J., Ulbrich, I. M., DeCarlo, P. F., Sueper, D., Jayne, J. T., Worsnop, D. R., Ziemann, P. J. and Jimenez, J. L.: Chemically-resolved aerosol volatility measurements from two megacity field studies, Atmos. Chem. Phys., 9, 7161–7182, 2009.

Huffman, J. A., Jayne, J. T., Drewnick, F., Aiken, A. C., Onasch, T., Worsnop, D. R. and Jimenez, J. L.: Design, modeling, optimization, and experimental tests of a particle beam width probe for the aerodyne aerosol mass spectrometer, Aerosol Sci. Technol., 39, 1143–1163, doi:10.1080/02786820500423782, 2005.

Jeong, C. H., Hopke, P. K., Kim, E. and Lee, D. W.: The comparison between thermal-optical transmittance elemental carbon and Aethalometer black carbon measured at multiple monitoring sites, Atmos. Environ., 38, 5193–5204, doi:10.1016/j.atmosenv.2004.02.065, 2004.

Kondo, Y., Matsui, H., Moteki, N., Sahu, L., Takegawa, N., Kajino, M., Zhao, Y., Cubison, M. J., Jimenez, J. L., Vay, S., Diskin, G. S., Anderson, B., Wisthaler, A., Mikoviny, T., Fuelberg, H. E., Blake, D. R., Huey, G., Weinheimer, A. J., Knapp, D. J. and Brune, W. H.: Emissions of black carbon, organic, and inorganic aerosols from biomass burning in North America and Asia in 2008, J. Geophys. Res., 116(D8), D08204, doi:10.1029/2010JD015152, 2011.

Laborde, M., Mertes, P., Zieger, P., Dommen, J., Baltensperger, U. and Gysel, M.: Sensitivity of the Single Particle Soot Photometer to different black carbon types, Atmos. Meas. Tech., 5(5), 1031–1043, doi:10.5194/amt-5-1031-2012, 2012a.

Laborde, M., Schnaiter, M., Linke, C., Saathoff, H., Naumann, K.-H., Möhler, O., Berlenz, S., Wagner, U., Taylor, J. W., Liu, D., Flynn, M., Allan, J. D., Coe, H., Heimerl, K., Dahlkötter, F., Weinzierl, B., Wollny, A. G., Zanatta, M., Cozic, J., Laj, P., Hitzenberger, R., Schwarz, J. P. and Gysel, M.: Single Particle Soot Photometer intercomparison at the AIDA chamber, Atmos. Meas. Tech., 5(12), 3077–3097, doi:10.5194/amt-5-3077-2012, 2012b.

Lack, D. A., Cappa, C. D., Covert, D. S., Baynard, T., Massoli, P., Sierau, B., Bates, T. S., Quinn, P. K., Lovejoy, E. R. and Ravishankara, A. R.: Bias in filter-based aerosol light absorption

measurements due to organic aerosol loading: Evidence from ambient measurements, Aerosol Sci. Technol., 42, 1033–1041, doi:10.1080/02786820802389277, 2008.

Langridge, J. M., Lack, D., Brock, C. A., Bahreini, R., Middlebrook, A. M., Neuman, J. A., Nowak, J. B., Perring, A. E., Schwarz, J. P., Spackman, J. R., Holloway, J. S., Pollack, I. B., Ryerson, T. B., Roberts, J. M., Warneke, C., de Gouw, J. A., Trainer, M. K. and Murphy, D. M. C.-D.: Evolution of aerosol properties impacting visibility and direct climate forcing in an ammonia-rich urban environment, J. Geophys. Res., 117, doi:10.1029/2011jd017116, 2012.

Liggio, J., Gordon, M., Smallwood, G., Li, S.-M., Stroud, C., Staebler, R., Lu, G., Lee, P., Taylor, B. and Brook, J. R.: Are emissions of black carbon from gasoline vehicles underestimated? Insights from near and on-road measurements., Environ. Sci. Technol., 46(9), 4819–28, doi:10.1021/es2033845, 2012.

McMeeking, G. R., Hamburger, T., Liu, D., Flynn, M., Morgan, W. T., Northway, M., Highwood, E. J., Krejci, R., Allan, J. D., Minikin, A. and Coe, H.: Black carbon measurements in the boundary layer over western and northern Europe, Atmos. Chem. Phys., 10(19), 9393–9414, doi:10.5194/acp-10-9393-2010, 2010.

Metcalf, A. R., Craven, J. S., Ensberg, J. J., Brioude, J., Angevine, W., Sorooshian, A., Duong, H. T., Jonsson, H. H., Flagan, R. C. and Seinfeld, J. H. C.-D.: Black carbon aerosol over the Los Angeles Basin during CalNex, J. Geophys. Res., 117, doi:10.1029/2011jd017255, 2012.

Moteki, N. and Kondo, Y.: Effects of mixing state on black carbon measurements by laser-induced incandescence, Aerosol Sci. Technol., 41, 398–417, doi:10.1080/02786820701199728, 2007.

Moteki, N. and Kondo, Y.: Dependence of Laser-Induced Incandescence on Physical Properties of Black Carbon Aerosols: Measurements and Theoretical Interpretation, Aerosol Sci. Technol., 44(8), 663–675, doi:10.1080/02786826.2010.484450, 2010.

Moteki, N., Kondo, Y., Oshima, N., Takegawa, N., Koike, M., Kita, K., Matsui, H. and Kajino, M.: Size dependence of wet removal of black carbon aerosols during transport from the boundary layer to the free troposphere, Geophys. Res. Lett., 39(13), L13802, doi:10.1029/2012GL052034, 2012.

Ng, N. L., Canagaratna, M. R., Zhang, Q., Jimenez, J. L., Tian, J., Ulbrich, I. M., Kroll, J. H., Docherty, K. S., Chhabra, P. S., Bahreini, R., Murphy, S. M., Seinfeld, J. H., Hildebrandt, L., Donahue, N. M., DeCarlo, P. F., Lanz, V. A., Prevot, A. S. H., Dinar, E., Rudich, Y. and Worsnop, D. R.: Organic aerosol components observed in Northern Hemispheric datasets from Aerosol Mass Spectrometry, Atmos. Chem. Phys., 10, doi:10.5194/acp-10-4625-2010, 2010.

Onasch, T. B., Trimborn, A., Fortner, E. C., Jayne, J. T., Kok, G. L., Williams, L. R., Davidovits, P. and Worsnop, D. R.: Soot Particle Aerosol Mass Spectrometer: Development, Validation, and Initial Application, Aerosol Sci. Technol., 46, 804–817, doi:10.1080/02786826.2012.663948, 2012.

Perring, A. E., Schwarz, J. P., Spackman, J. R., Bahreini, R., de Gouw, J. A., Gao, R. S., Holloway, J. S., Lack, D. A., Langridge, J. M., Peischl, J., Middlebrook, A. M., Ryerson, T. B., Warneke, C., Watts, L. A. and Fahey, D. W.: Characteristics of black carbon aerosol from a surface oil burn during the Deepwater Horizon oil spill, Geophys. Res. Lett., 38, doi:L17809 10.1029/2011gl048356, 2011.

Sahu, L. K., Kondo, Y., Moteki, N., Takegawa, N., Zhao, Y., Cubison, M. J., Jimenez, J. L., Vay, S., Diskin, G. S., Wisthaler, A., Mikoviny, T., Huey, L. G., Weinheimer, A. J. and Knapp, D. J.: Emission characteristics of black carbon in anthropogenic and biomass burning plumes over California during ARCTAS-CARB 2008, J. Geophys. Res., 117(D16), D16302, doi:10.1029/2011JD017401, 2012.

Schnaiter, M., Linke, C., Mohler, O., Naumann, K. H., Saathoff, H., Wagner, R., Schurath, U. and Wehner, B. C.-D.: Absorption amplification of black carbon internally mixed with secondary organic aerosol, J. Geophys. Res., 110, doi:10.1029/2005jd006046, 2005.

Schwarz, J. P., Gao, R. S., Spackman, J. R., Watts, L. A., Thomson, D. S., Fahey, D. W., Ryerson, T. B., Peischl, J., Holloway, J. S., Trainer, M., Frost, G. J., Baynard, T., Lack, D. A., de Gouw, J. A., Warneke, C. and Del Negro, L. A.: Measurement of the mixing state, mass, and optical size of individual black carbon particles in urban and biomass burning emissions, Geophys. Res. Lett., 35(13), L13810, doi:10.1029/2008GL033968, 2008a.

Schwarz, J. P., Spackman, J. R., Fahey, D. W., Gao, R. S., Lohmann, U., Stier, P., Watts, L. A., Thomson, D. S., Lack, D. A., Pfister, L., Mahoney, M. J., Baumgardner, D., Wilson, J. C. and Reeves, J. M. C.-D.: Coatings and their enhancement of black carbon light absorption in the tropical atmosphere, J. Geophys. Res., 113, doi:10.1029/2007jd009042, 2008b.

Schwarz, J. P., Spackman, J. R., Gao, R. S., Perring, A. E., Cross, E., Onasch, T. B., Ahern, A., Wrobel, W., Davidovits, P., Olfert, J., Dubey, M. K., Mazzoleni, C. and Fahey, D. W.: The Detection Efficiency of the Single Particle Soot Photometer, Aerosol Sci. Technol., 44(8), 612–628, doi:10.1080/02786826.2010.481298, 2010.

Schwarz, J. P., Stark, H., Spackman, J. R., Ryerson, T. B., Peischl, J., Swartz, W. H., Gao, R. S., Watts, L. A. and Fahey, D. W. C.-L.: Heating rates and surface dimming due to black carbon aerosol absorption associated with a major US city, Geophys. Res. Lett., 36, doi:10.1029/2009gl039213, 2009.

Shiraiwa, M., Kondo, Y., Moteki, N., Takegawa, N., Sahu, L. K., Takami, A., Hatakeyama, S., Yonemura, S. and Blake, D. R.: Radiative impact of mixing state of black carbon aerosol in Asian outflow, J. Geophys. Res., 113, doi:10.1029/2008jd010546, 2008.

Slowik, J. G., Cross, E. S., Han, J. H., Davidovits, P., Onasch, T. B., Jayne, J. T., Williams, L. R., Canagaratna, M. R., Worsnop, D. R., Chakrabarty, R. K., Moosmuller, H., Arnott, W. P., Schwarz, J. P., Gao, R. S., Fahey, D. W., Kok, G. L. and Petzold, A.: An inter-comparison of instruments measuring black carbon content of soot particles, Aerosol Sci. Technol., 41, 295–314, doi:10.1080/02786820701197078, 2007.

Subramanian, R., Kok, G. L., Baumgardner, D., Clarke, A., Shinozuka, Y., Campos, T. L., Heizer, C. G., Stephens, B. B., de Foy, B., Voss, P. B. and Zaveri, R. A.: Black carbon over Mexico: the effect of atmospheric transport on mixing state, mass absorption cross-section, and BC/CO ratios, Atmos. Chem. Phys., 10, 219–237, 2010.

Zhang, X., Lin, Y.-H., Surratt, J. D., Zotter, P., Prevot, A. S. H. and Weber, R. J. C.-L.: Light-absorbing soluble organic aerosol in Los Angeles and Atlanta: A contrast in secondary organic aerosol, Geophys. Res. Lett., 38, doi:10.1029/2011gl049385, 2011.